Probe Compensated Single Feed Circularly Polarized Fractal-Shaped Microstrip Antennas

P. Nageswara Rao, N. V. S. N. Sarma

Department of Electronics and Communications Engineering, National Institute of Technology, Warangal, India

Received 16 January 2009; accepted 14 April 2009

ABSTRACT: A single feed circularly polarized fractal boundary microstrip antenna with improved axial ratio bandwidth is presented. The low-axial ratio bandwidth of single feed circularly polarized microstrip antenna is due to its probe reactance. In this article, the inherent disadvantage of this low-AR bandwidth is overcome by compensating the probe reactance by incorporating capacitance in the form of small patch between the radiating patch and the probe. The perturbation of the patch is done using fractal curve as boundary. The proposed antenna exhibits impedance and axial ratio bandwidths of 9 and 2.2% respectively at 2.4 GHz. © 2009 Wiley Periodicals, Inc. Int J RF and Microwave CAE 19: 647–656, 2009.

Keywords: fractal boundary; Minkowski; Koch; axial ratio; circular polarization; probe compensation

I. INTRODUCTION

The application of fractal geometry in the design of microstrip antennas is a recent technique to get the benefits of compact size, high bandwidth, multiband operation, etc. There have been a number of research articles available on these fractal geometries to design microstrip and wire antennas for the last one decade. An excellent review on fractal antennas is given by Werner and Ganguly in [1]. Gianvittorio and Rahmat-Samii [2] presented the use of Minkowski and Koch island curves in the design of loop antennas and shown that the resonant frequency can be systematically changed by varying the indentation depth of the Minkowski curve. A fractal-shaped small size microstrip antenna using Koch curve is described by Kim et al. [3]. The behavior of Koch fractal curves with different indentation angles and relationship between the fractal dimension of the Koch curves and their resonant frequency is demonstrated by Vinoy et al. [4]. After thoroughly going through the literature, it is observed that the fractal geometry can be used to design circularly polarized microstrip antennas because of its geometrical flexibility.

Many articles are available in the open literature on single feed circularly polarized microstrip antennas. The simplest and foremost single feed circularly polarized microstrip antenna is reported by Sharma and Guptha [5] using a nearly square patch and truncated square patch antennas. A dual band circularly polarized square microstrip antenna with 3 dB axial ratio bandwidth about 1% is presented by Yang and Wong [6]. Circularly polarized single Fed wide band microstrip antenna is reported by Naftali Herscovici et al. [7] with 3 dB axial ratio bandwidth of 13%. Nevertheless, the thickness of the substrate is 13.4 mm with stacked configuration. Sudha et al. [8] presented a wide band single fed circularly polarized patch antenna using three-layered stacked patch antenna. A small circularly polarized patch antenna is discussed by Wong et al. [9] with 3 dB axial ratio

Correspondence to: N. Rao; e-mail: nrraop@yahoo.com
DOI 10.1002/mmce.20388
Published online 13 July 2009 in Wiley InterScience (www.interscience.wiley.com).

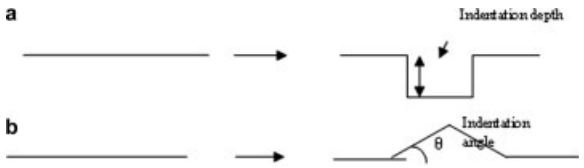

Figure 1. Generation of (a) Minkowski fractal curve (b) Koch fractal curve.

bandwidth of 0.381%. Lee and Nalbandian [10] demonstrated the operation of planar circularly polarized microstrip antenna using double layer structure by providing two coupling holes in the lower patch to obtain 6 dB axial ratio bandwidth of 2.4 %. Wong and Lin [11] presented a circularly polarized microstrip antenna with tuning stub to a circular patch having the 3 dB axial ratio band width of about 0.9%. A compact single feed circularly polarized circular patch antenna with crossed slots on both radiating patch and ground plane is reported by Row and Ai [12] with 3 dB axial ratio bandwidth of around 1%. Wong and Wu [13] described a single feed cp square patch antenna by providing four slits on the sides of the patch with 1.3% axial ratio bandwidth. A novel compact circularly polarized square microstrip antenna is reported by Chen et al. [14] with 3 dB axial ratio bandwidth of about 0.8%. A single feed square ring microstrip antenna with truncated corners for compact cp operation is presented by Chen et al. [15] with cp bandwidth around 1.3%. Lu et al. [16–20] reported several variations of equilateral triangular patch antenna for cp operation with 3 dB axial ratio bandwidth around 1%.

In this article, a novel technique is adopted to obtain circular polarization using prefractal curves like Minkowski and Koch as boundaries to the square patch to perturb the patch configuration. Both impedance and cp bandwidth are improved remarkably by introducing a small capacitance in series with the probe to compensate the probe reactance.

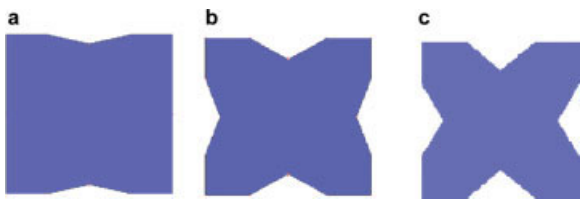

Figure 2. Geometry fractal boundary cp antennas: (a) Koch Antenna 1, (b) Koch antenna 2, (c) Koch antenna 3, and (d) Koch antenna 4. [Color figure can be viewed in the online issue, which is available at www.interscience.wiley.com.]

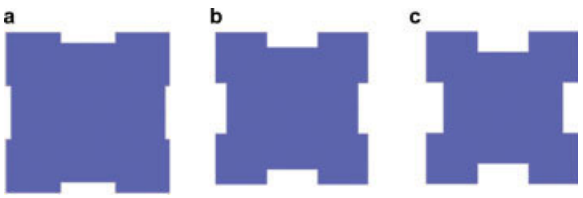

Figure 3. Geometry of fractal boundary antennas (a) Minkow antenna 1, (b) Minkow antenna 2, and (c) Minkow antenna 3. [Color figure can be viewed in the online issue, which is available at www.interscience.wiley.com.]

II. FRACTAL DIMENSION OF FRACTAL CURVE

Fractal dimension can be defined as a measure of space filling ability of a fractal shape. For the Euclidean shapes, a cube fully occupies three dimensions, a flat plate completely fills two dimensions and a line fills one dimension. There are different versions of fractal dimension available in the literature. The self-similarity dimension is one among them [2]. The generation of the Minkowski fractal curve is shown in Figure 1a. The prefractal curve is obtained by dividing the line into three equal parts and the middle third is replaced by some fraction of 1/3. This is called indentation depth "d," which can vary from 0 to 1. The resulting structure has five segments and the length of curve is increased by a factor (1 + 2*d/3). The fractal dimension of Minkowski curve can be found by solving the following eq. (1).

$$k_1\left(\frac{1}{h_1}\right)^{\mathrm{D}} + k_2\left(\frac{1}{h_2}\right)^{\mathrm{D}} = 1 \qquad (1)$$

The subscripts are required to differentiate between the two scales present in the generating iterations. Where k_n represents the number of copies of the initiator scaled by h_n. $k_1 = 3$ and $h_1 = 3$ will be representing the horizontal segments whereas $k_2 = 2$ and $h_2 = 3/d$, represent the vertical segments. Similarly, the generation of the Koch curve is shown in Figure 1b. It starts with a straight line called the initiator, this is partitioned into three equal parts, and the segment at the middle is replaced with two others of same length. This is the first iterated one and similar process can be applied to get the higher iterations. The self-similarity dimension of the Koch curve is defined as [4]

$$D = \frac{\log n}{\log\left(\frac{1}{s}\right)} \qquad (2)$$

TABLE I. Koch Fractal Boundary cp Antennas and Their Resonant Frequencies Corresponding to TM_{10} and TM_{01} Modes (Measured)

Antenna	Indentation Angle Along *x*- and *y*-Directions (°)		Fractal Dimension Along *x*- and *y*-Directions		fr (TM_{10}mode) (MHz)	fr (TM_{01}mode) (MHz)	Center Frequency (MHz)
Koch antenna 1	13	0	1.0094	1	2580	2460	2510
Koch antenna 2	30	20	1.0526	1.0225	2520	2440	2472
Koch antenna 3	40	31	1.0985	1.0564	2480	2400	2426
Koch antenna 4	50	43	1.1650	1.1160	2380	2320	2343

where D is the fractal dimension, n is the number copies, and s is the scaling factor. Then, the resulting structure has four segments and length of the curve is increased by a factor 4/3. Instead of taking indentation angle as 60°, if any other angle θ is taken, the generalized Koch curve can be obtained. Then the self-similarity dimension of the generalized Koch curve is given by

$$D = \frac{\log 4}{\log[2(1 + \cos\theta)]} \tag{3}$$

The resulting structure has four segments, and the length of the curve is increased by a factor 4/[2(1 + cos θ)] instead of 4/3. As circular polarization is mainly based on excitation of two orthogonal modes, it is required to have two different resonant lengths in two directions of the patch. The fractal dimension of the fractal curve facilitates to choose different electrical lengths in two directions of the patch. In the case of Minkowski fractal curve as boundary, indentation depth factor is the parameter which changes the electrical length and in the case of Koch curve as the boundary to the square patch indentation angle is the parameter to change the electrical length. This plays a key role in getting circular polarization with fractal curve as boundary because fractal dimension can be changed just by changing the depth factor or indentation angle.

III. cp OPERATION WITH FRACTAL BOUNDARY PATCH ANTENNAS

The four sides of square patch are replaced by Minkowski and Koch fractal curves of first/second iteration with different fractal dimensions while keeping equal dimension for opposite sides. To obtain cp with single feed, it is required to excite two orthogonal near degenerate modes within the patch. This dictates the electrical length in two perpendicular directions of the patch to be slightly different. Figures 2 and 3 illustrate the Koch and Minkowski fractal boundary cp antennas with different indentation angles and indentation depth factors along *x*- and *y*-directions of the patch to get circular polarization. The initial side length of all the patches in this paper is 36.4 mm and are printed on RT Duroid substrate having dielectric constant 2.33 with thickness 3.2 mm. Equations (1) and (3) are used to evaluate the fractal dimensions of the Minkowski and Koch fractal boundary cp antennas. The resonant frequencies corresponding to TM_{10} and TM_{01} are obtained by feeding the antennas along *y*- and *x*-axis, respectively. The center frequency is the frequency corresponding to the minimum axial ratio when the antenna is fed along the diagonal. The details are given in Tables I and II. The measured S11 characteristics for both the antennas are shown in Figures 4 and 5.

When the Euclidean sides of square patch are replaced by Koch and Minkowski with indentation

TABLE II. Minkowski Fractal Boundary cp Antennas and Their Resonant Frequencies Corresponding to TM_{10} and TM_{01} Modes (Measured)

Antenna	Indentation Depth Factor Along *x*- and *y*-Directions		Fractal Dimension Along *x*- and *y*-Directions		fr (TM_{10}mode) (MHz)	fr (TM_{01}mode) (MHz)	Center Frequency (MHz)
Minkow antenna 1	0.15	0.03	1.076	1.0163	2564	2456	2486
Minkow antenna 2	0.23	0.12	1.112	1.062	2544	2444	2475
Minkow antenna 3	0.3	0.2	1.1419	1.0952	2512	2416	2446

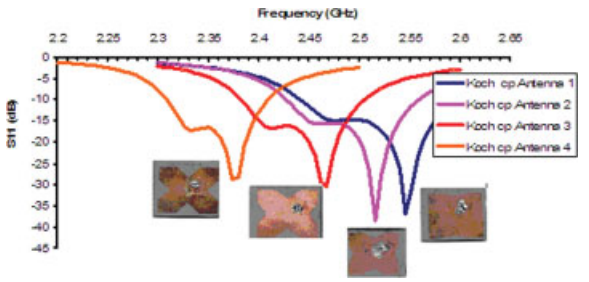

Figure 4. Measured S11 characteristics of Koch fractal boundary cp antenna for different cases. Koch antenna 1 (13°, 0°), Koch cp antenna 2 (30°, 20°), Koch cp antenna 3 (40°, 31°), and Koch antenna 4 (50°, 43°). Photographs of the fabricated antennas are also shown in the graph. [Color figure can be viewed in the online issue, which is available at www.interscience.wiley.com.]

angle "θ" and depth factor "d," respectively, then the corresponding lengths are increased by factors (2/(1 + cos θ)) and (1 + 2*d/3). As the θ and d are chosen differently in two sides the aspect ratio becomes slightly greater than one. This makes the antenna to provide circular polarization, because whenever the aspect ratio is slightly greater than "1" the required two orthogonal modes will be excited. For Minkowski cp antenna, the aspect ratio should be within 1.017 and 1.07 and for Koch cp it should be within 1.012 and 1.053 to excite two orthogonal modes with thickness 3.2 mm and dielectric constant 2.33. The limits of aspect ratio may be changed when the thickness and ε_r are changed.

The measured and simulated axial ratio characteristics of cp antenna operating at 2510 MHz is shown in Figure 6. The measured radiation pattern and rotating linear pattern of the antenna is shown in Figures 7a and 7b. The width between the two curves on the radiation pattern is equal to the axial ratio in that

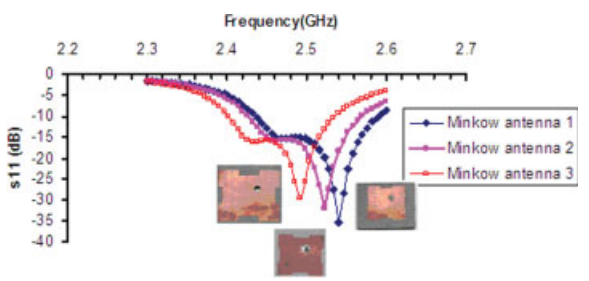

Figure 5. Measured S11 characteristics of Minkowski fractal boundary cp antennas for different indentation depth factors Minkow antenna 1 (0.15, 0.03), Minkow Antenna 2 (0.23, 0.12), and Minkow antenna 3 (0.3, 0.2). Photographs of the fabricated antennas are also shown in the graph. [Color figure can be viewed in the online issue, which is available at www.interscience.wiley.com.]

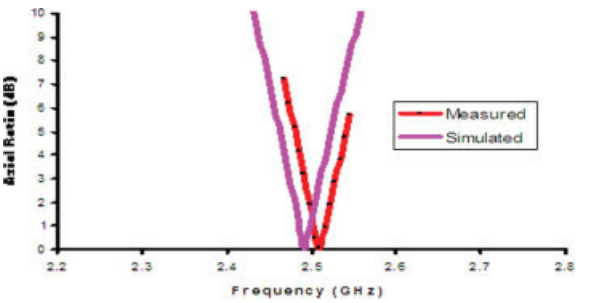

Figure 6. Measured and simulated axial ratio characteristics of Koch cp antenna 1. [Color figure can be viewed in the online issue, which is available at www.interscience.wiley.com.]

direction. From the rotating linear pattern, it is clearly seen that the axial ratio in the bore sight direction is close to 0 dB.

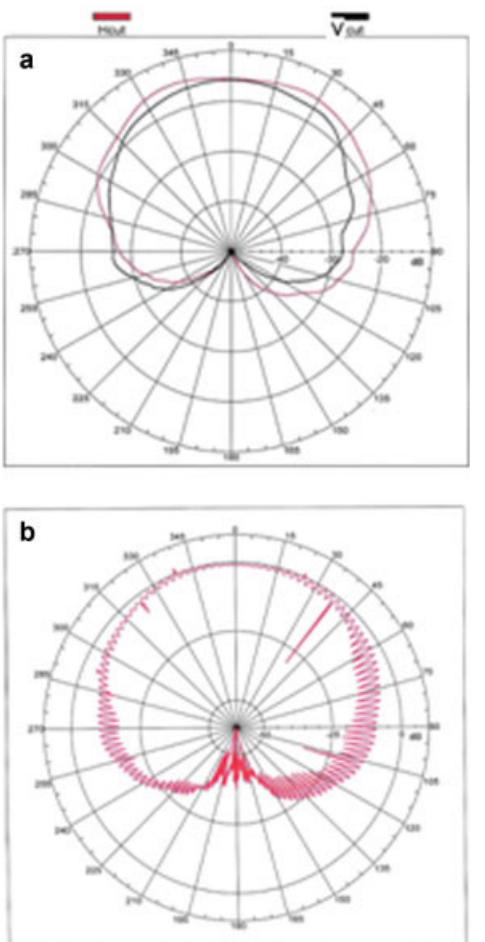

Figure 7. Measured (a) radiation pattern and (b) rotating linear pattern of Koch fractal boundary cp antenna operating at 2510 MHz. [Color figure can be viewed in the online issue, which is available at www.interscience.wiley.com.]

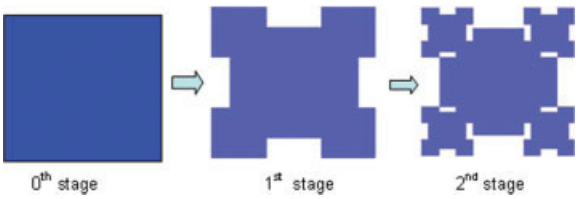

Figure 8. The generation of second stage Minkowski cp antenna. [Color figure can be viewed in the online issue, which is available at www.interscience.wiley.com.]

A. Second Stage Minkowski cp Antenna

The generation of second stage Minkowski fractal boundary cp antenna is shown in Figure 8.

When the opposite pairs of square patch are replaced by Minkowski fractal curve of second stage with depth factors d_1 and d_2 as shown in Figure 9, their electrical lengths are increased by a factor as given in eqs. (4) and (5).

$$b = L^*\left[1 + \left(\frac{2}{3}\right)^n * d_1\right] \tag{4}$$

and

$$a = L^*\left[1 + \left(\frac{2}{3}\right)^n * d_2\right] \tag{5}$$

where "b" and "a" are the side lengths on two opposite pairs of the patch and "n" is number of iterations. Although the sides are replaced by the fractal curves, the end to end dimension of the patch remains constant. As the depth factors are different in two

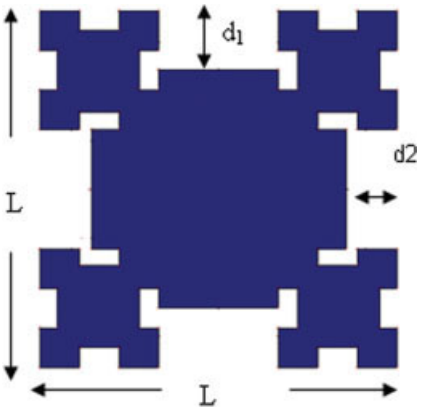

Figure 9. Second stage Minkowski fractal boundary cp antenna (L =36.4 mm). [Color figure can be viewed in the online issue, which is available at www.interscience.wiley.com.]

directions of the patch, the requisite two orthogonal modes are excited in the patch when the antenna is fed along the diagonal. The depth factor on one pair of sides can be fine tuned to excite two near degenerate modes while keeping the depth factor constant on the other two sides. As long as the aspect ratio (b/a) is with in the certain limits cp is always possible. The aspect ratio should be in between 1.012 and 1.028 for the second iterated Minkowski cp antenna. As seen from Tables III and IV, the resonant frequency of the Minkowski cp antenna is changed from 2481 to 2106 MHz when the depth factor is varied from 0. 2 to 0.7 for the first iterated one, whereas for the second iterated one it is changed from 2196 to 2023 MHz when the depth factor is changed from 0.4180 to 0.7. As fractal boundaries are used obvi-

TABLE III. Summary of Results of Minkowski Fractal Boundary cp Antenna—Stage 1 (Simulated)

Antenna	Depth Factor (d_1)	Physical Length (b) (mm)	Depth Factor (d_2)	Physical Length (a) (mm)	Aspect Ratio (b/a)	f_0 (MHz)
Antenna 1	0.2	41.25	0.09	38.584	1.069	2481
Antenna 2	0.3	43.68	0.2063	41.4	1.055	2447
Antenna 3	0.4	46.1	0.3263	44.31	1.04	2387
Antenna 4	0.5	48.53	0.4395	47.0652	1.0311	2307
Antenna 5	0.6	50.96	0.555	49.868	1.0289	2217
Antenna 6	0.7	53.38	0.6618	52.45	1.017	2106

TABLE IV. Summary of the Results of Stage 2 Minkowski Fractal Boundary cp Antenna (Simulated)

Antenna	Depth Factor (d_1)	Physical Length (b) (mm)	Depth Factor (d_2)	Physical Length (a) (mm)	Aspect Ratio (b/a)	f_0 (MHz)
Antenna 1	0.4180	43.08	0.34	41.9	1.028	2196
Antenna 2	0.5	44.48	0.4315	43.38	1.025	2159
Antenna 3	0.6	46.1	0.5472	45.25	1.018	2101
Antenna 4	0.7	47.72	0.66273	47.12	1.012	2023

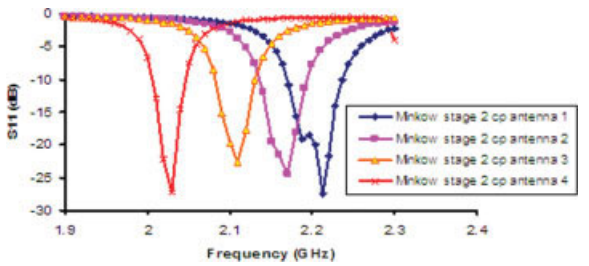

Figure 10. S11 characteristics of Minkowski stage 2 cp antennas (simulated). [Color figure can be viewed in the online issue, which is available at www.interscience.wiley.com.]

ously the size of the patch is reduced compared with the conventional antennas. Generally, the size of the antenna is $\approx\lambda_g/2$, but here the antenna occupies only 0.46 to 0.37 λ_g (Ex. The antenna size is only 0.428 λ_g operating at 2310 MHz). Figure 10 shows the return loss characteristics of Minkowski cp antenna stage-2.

IV. PROBE COMPENSATED FRACTAL-SHAPED cp ANTENNAS

The impedance and cp bandwidths obtained are about 5 and 1.6% respectively with the method presented [21, 22]. These low bandwidths are because of inductance of the coaxial probe which is used to feed the antenna. So an obvious approach to improve the bandwidth is to tune out this inductance with a series capacitor. One way of implementing this technique is

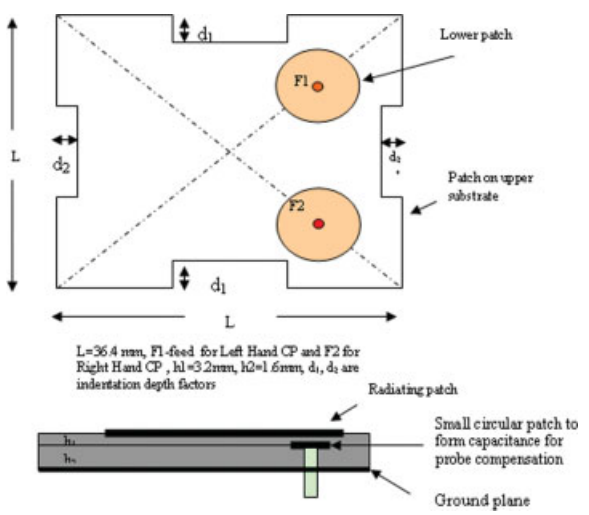

Figure 11. Antenna geometry and feed structure for the probe compensated case. [Color figure can be viewed in the online issue, which is available at www.interscience.wiley.com.]

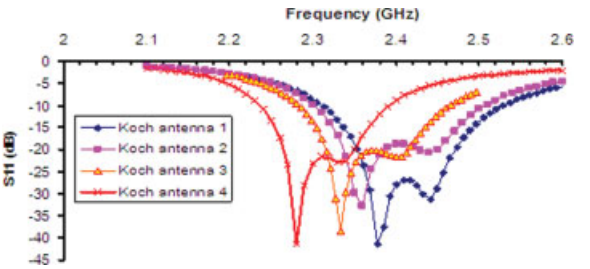

Figure 12. Simulated S11 characteristics Koch fractal boundary cp antennas for different indentation angles with probe reactance compensated. Koch antenna 1 (20, 0), Koch antenna 2 (30, 11); Koch antenna 3 (40, 25), and Koch antenna 4 (50, 36). [Color figure can be viewed in the online issue, which is available at www.interscience.wiley.com.]

to form a tab at one end of the coaxial feed that does not directly contact the patch element [23]. With this technique, it is shown in this article that the impedance and axial ratio bandwidth are increased to reasonably high values. To have a tab at the end of coaxial probe a small circular patch of 6–8 mm radius is used, to which the probe is connected directly. This small circular shaped patch is printed on a substrate of thickness 3.2 mm with dielectric constant 2.33 and the radiating patch is printed on a substrate with thickness of 1.6 mm having dielectric constant of 2.33. As the probe is not directly connected to the radiating patch, a small capacitance is formed between the radiating patch and the probe. The geometry of the probe compensated antenna is shown in Figure 11. The radius of the circular patch is chosen such that, the capacitive reactance of capacitor so formed will nullify the inductive reactance of the probe. All the simulations are done using Zeland IE3D electromagnetic simulator [24]. Figures 12–15 show the characteristics of the said antennas with

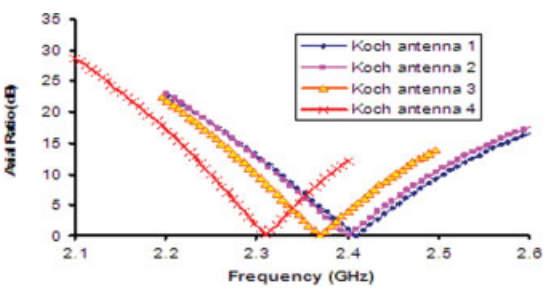

Figure 13. Axial ratio versus frequency of Koch fractal boundary cp antennas for different indentation angles with probe compensated (simulated). [Color figure can be viewed in the online issue, which is available at www.interscience.wiley.com.]

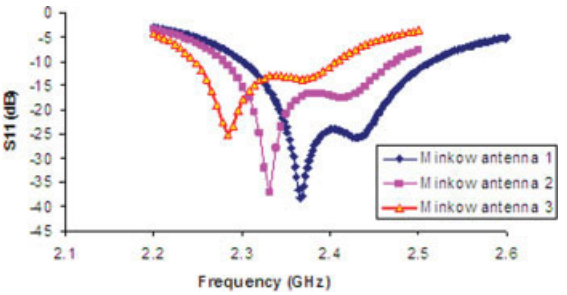

Figure 14. Simulated S11 characteristics of Minkowski fractal boundary cp antennas for different indentation depth factors with probe compensation. Minkow antenna 1 (0.2, 0.09), Minkow antenna 2 (0.3, 0.132), and Minkow antenna 3 (0.4, 0.266). [Color figure can be viewed in the online issue, which is available at www.interscience. wiley.com.]

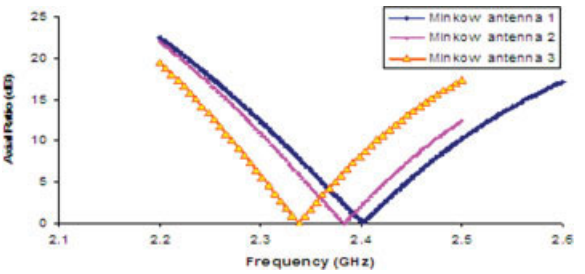

Figure 15. Axial ratio versus frequency of Minkowski fractal boundary cp antennas for different indentation depth factors with probe compensation (simulated). [Color figure can be viewed in the online issue, which is available at www.interscience.wiley.com.]

probe compensation. By observing the characteristics it is clearly seen that both the impedance and axial ratio bandwidths are increased.

The details are listed in Tables V and VI. One can observe that for the antenna operating at 2.5 GHz the impedance bandwidth is increased from 6.2 to 9.05% and 3 dB axial ratio bandwidth is increased from 1.6 to 2.2% with the probe compensation. With this method, it is also possible to get polarization agility as the feed can be changed easily to the other diagonal because the probe is not connected directly to the radiating patch. With the feed position F1 indicated in Figure 11 on the top gives left hand circular polarization, whereas the feed F2 on the other diagonal gives right hand circular polarization. Further, the co- and cross-polarization levels are well isolated. The axial ratio bandwidth can be improved only when the impedance bandwidth is increased, because the axial ratio bandwidth of circularly polarized antenna is less than half the impedance bandwidth of corresponding

TABLE V. Impedance and Axial Ratio Band Width Comparison for the Probe Uncompensated and Compensated Koch Fractal Boundary cp Antennas

Antenna (Koch Fractal Boundary)	Thickness of Substrate-Including Capacitive Tab (λ_g)		Center Frequency (MHz)		10 dB imp BW (%)		3 dB Axial Ratio BW (%)	
	A	B	A	B	A	B	A	B
Antenna 1	0.0408	0.0588	2510	2408	6.2	9.05	1.6	2.2
Antenna 2	0.0402	0.0586	2472	2402	5.25	8.7	1.3	2.04
Antenna 3	0.0395	0.0578	2426	2370	4.98	7.7	1.2	1.9
Antenna 4	0.0381	0.0564	2343	2310	4.26	6.75	1	1.68

A: Antenna without probe compensation; B: Antenna with probe compensation.

TABLE VI. Impedance and Axial Ratio Band Width Comparison for the Probe Uncompensated and Compensated Minkowski Fractal Boundary cp Antennas

Antenna (Minkowski Fractal Boundary)	Thickness of Substrate (λ_g)-Including Capacitive Tab		Center Frequency (MHz)		10 dB imp BW (%)		3 dB Axial Ratio BW (%)	
	A	B	A	B	A	B	A	B
Antenna 1	0.0404	0.0586	2486	2402	6.1	8.78	1.45	2.12
Antenna 2	0.0403	0.0581	2475	2381	5.7	8.23	1.37	2.01
Antenna 3	0.0398	0.0572	2446	2343	5.43	6.95	1.27	1.74

A: Antenna without probe compensation; B: Antenna with probe compensation.

linearly polarized antenna and the impedance bandwidth of circularly polarized antenna is twice that of corresponding linearly polarized antenna for typical values of AR_{max} and $VSWR_{max}$ [25]. For typical values of AR_{max}= 3db and $VSWR_{max}$ = 2, the

$$BW_{cp}^{AR} \approx 0.338/Q \quad (6)$$

$$BW_{LP}^{IMP} \approx 0.707/Q \quad (7)$$

$$BW_{cp}^{IMP} \approx 1.414/Q \quad (8)$$

From eqs. (6) to (8), it can be inferred that the proposed method for improving the AR bandwidth is justified.

To observe how much improvement is obtained with probe compensation, the return loss characteristics of Minkowski fractal boundary cp antenna with indentation depth factor of 0.5 for both the cases are plotted. From Figure 16, it is clear that the impedance bandwidth is increased from 90 to 130 MHz, apart from shifting of resonance frequency toward the origin. As impedance bandwidth is increased it is expected that the 3 dB axial ratio bandwidth will also be improved in the same proportion.

It is clear from the Table VII almost for the same size 3 dB AR bandwidth of the probe compensated cp antenna is better than the other published cp antennas.

The perfect circular polarization can be easily visualized with the help of impedance variation on the smith chart as shown in Figure 17, where the variation of input impedance contains a single loop of almost zero area [26]. Because of the reactance of the probe, at the center frequency the curve is not on the real-axis for the case of without probe compensation whereas the curve is almost at the center of the smith chart for the case of probe compensation because the reactance is tuned out. If thicker substrate is used without the capacitance tab same bandwidth can be obtained, but the antenna efficiency will be lowered.

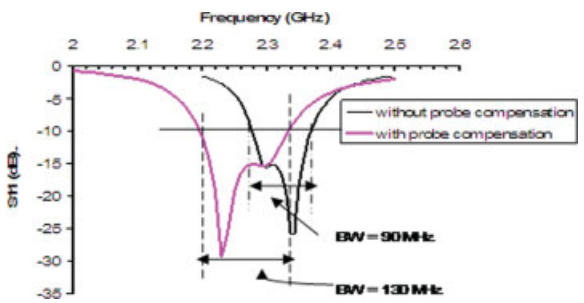

Figure 16. Impedance bandwidth comparison for the two cases of Minkowski fractal boundary cp antenna with indentation depth factor 0.5 (simulated). [Color figure can be viewed in the online issue, which is available at www.interscience.wiley.com.]

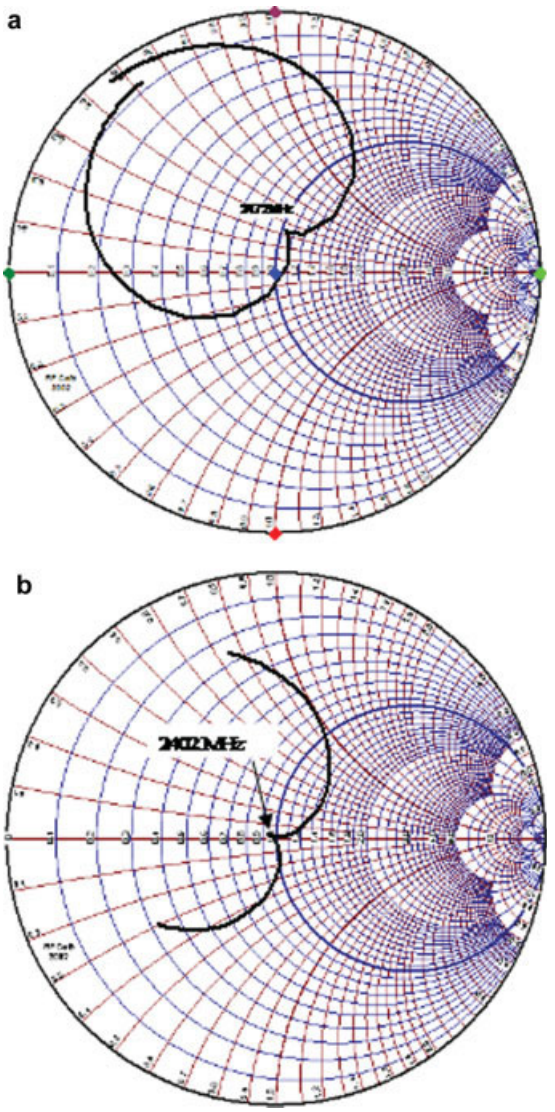

Figure 17. Variation of input impedance of Koch fractal boundary cp antenna-2 (a) without probe compensation and (b) with probe compensation. [Color figure can be viewed in the online issue, which is available at www.interscience.wiley.com.]

V. CONCLUSION

A probe compensated single feed circularly polarized fractal boundary microstrip antenna is presented. It is established that by using a small circular shaped patch between the probe and the radiating patch with

TABLE VII. Comparison of Various Parameters of Published cp Antennas with the Proposed Probe Compensated cp Antenna

Published Data	Size of the Antenna (λ_g)	Electrical Thickness (λ_g)	AR Bandwidth (%)
This article (antenna 1 in Table V)	0.446	0.0588	2.2 (3 dB BW)
[5] Nearly square	0.437	0.0525	1.086 (6dB BW)
[5] Truncated corners	0.459	0.0538	0.831 (6 dB BW)
[5] Diagonal slot	0.4312	0.053	1.134 (6 dB BW)
[6]	0.4302	0.0172	1.17 (3 dB BW)
[10]	0.58	0.0413	2.4 (6 dB BW)
[13]	0.466	0.0249	1.62 (3 dB BW)
[14]	0.443	0.0253	0.84 (3 dB BW)
[15]	0.456	0.026	1.37 (3dB BW)

a small gap to tune out the probe reactance, the impedance and axial ratio bandwidths can be improved. Comparison is made between probe compensated and directly fed patch antennas in respect of impedance and axial ratio bandwidths. Many of the antennas (without probe compensation) have been fabricated and measured results are compared with simulated results and very good agreement is obtained between the results. It is also demonstrated that the perturbation of the patch with the help of fractal curves as boundary to the square patch gives good circular polarization. The proposed cp antenna is easy to fabricate, provides good circular polarization and occupies less space compared with the square patch. Hence, it can be one of the best candidates for GPS, PCS, PCN, RFID, and mobile satellite applications.

REFERENCES

1. D.H. Werner and S. Ganguly, An overview of fractal antenna engineering research, IEEE Antennas Propag Mag 45 (2003), 38–55.
2. J.P. Gianvittorio and Y.R. Samii, Fractal antennas: A novel antenna miniaturization technique and applications, IEEE Antennas Propag Mag 44 (2002), 20–36.
3. I.-K. Kim, J.-G. Yook, and H.-K. Park, Fractal shape small size microstrip patch antenna, Microwave Opt Technol Lett 34 (2002), 15–17.
4. K.J. Vinoy, J.K. Abraham, and V.K. Vardan, On the relationship between fractal dimension and the performance of multi-resonant dipole antennas using Koch curves, IEEE Trans Antennas Propag 51 (2003), 2296–2303.
5. P.C. Sharma and K.C. Guptha, Analysis and optimized design of single feed circularly polarized microstrip antenna, IEEE Trans Antennas Propag 31 (1983), 949–955.
6. K.-P. Yang and K.-L. Wong, Dual-band circularly-polarized square microstrip antenna, IEEE Trans Antennas Propag 49 (2001), 377–382.
7. N. Herscovici, Z. Sipus, and D. Bonefacic, Circularly polarized single-fed wide band microstrip patch, IEEE Trans Antennas Propag 51 (2003), 1277–1280.
8. T. Sudha, T.S. Vedhavathy, and N. Bhat, Wideband single fed circularly polarized patch antenna, Electron lett 40 (2004), 648–649.
9. M.L. Wong, H. Wong, and K.M. Luk, Small circularly polarized patch antenna, Electron Lett 41 (2005), 7–8.
10. C.S. Lee and V. Nalbandian, Planar circularly polarized microstrip antenna with a single feed, IEEE Trans Antennas Propag 47 (1999), 1005–1007.
11. K.-L. Wong and Y.-F. Lin, Circularly polarized microstrip antenna with a tuning stub, Electron Lett 34 (1998), 831–832.
12. J.S. Row and C.Y. Ai, Compact design of single feed circularly polarized microstrip antenna, Electron Lett 40 (2004), 1093–1094.
13. K.-L. Wong and J.-Y. Wu, Single feed small circularly polarized square microstrip antenna, Electron Lett 33 (1997), 1833–1834.
14. W.-S. Chen, C.-K. Wu, and K.L. Wong, Novel compact circularly polarized square microstrip antenna, IEEE Trans Antennas Propag 49 (2001), 340–342.
15. W.-S. Chen, C.-K. Wu, and K.-L. Wong, Single feed square-ring microstrip antenna with truncated corners for compact circular polarization operation, Electron Lett 34 (1998), 1045–1046.
16. J.-H. Lu, H.C. Yu, and K.-L. Wong, Compact circular polarization design for equilateral-triangular microstrip antenna with spur lines, Electron Lett 34 (1998), 1989–1990.
17. C.-L. Tang, J.-H. Lu, and K.L. Wong, Circularly polarized equilateral triangular microstrip antenna with truncated tip, Electron Lett 34 (1998), 1277–1278.
18. J.-H. Lu, C.-L. Tang, and K.L. Wong, Circular polarization design of a single feed equilateral triangular microstrip antenna, Electron Lett 34 (1998), 319–320.
19. J.-H. Lu, C.-L. Tang, and K.-L. Wong, Single feed slotted equilateral-triangular microstrip antenna for circular polarization, IEEE Trans Antennas Propag 47 (1999), 1174–1178.

20. J.-H. Lu and K.-L. Wong, Single-feed circularly polarized equilateral-triangular microstrip antenna with a tuning stub, IEEE Trans Antennas Propag 48 (2000), 1869–1872.
21. P.N. Rao and N.V.S.N. Sarma, Fractal boundary circularly polarized single feed microstrip antenna, Electron Lett 44 (2008), 713–714.
22. P.N. Rao and N.V.S.N. Sarma, Minkowski fractal boundary single feed circularly polarized microstrip antenna, Microwave Opt Technol Lett 50 (2008), 2820–2824.
23. F.S. Fong, H.F Pues, and M.J. Withers, Wideband multi layer coaxial fed microstrip antenna element, Electron Lett 21 (1985), 497–499.
24. R. James and P.S. Hall, Hand book of microstrip antennas, Vol. 1, Peter Peregrinus, Ltd., London, UK, 1989, pp. 232–233.
25. Available at: www.zeland.com
26. W.L. Langston and D.R. Jackson, Impedance, axial-ratio and receive-power bandwidth of microstrip antennas, IEEE Trans Antennas Propag 52 (2004), 2769–2773.

BIOGRAPHIES

P. Nageswara Rao received his B.Tech degree from Nagarjuna University, Guntur, India, in Electronics and Communications Engineering and Master's degree from Coimbatore Institute of Technology, Coimbatore, India, in 1990 and 1995, respectively. He worked as faculty in ECE department at NBKRIST, Nellore and Sree Vidyanikethan Engineering College, Tirupati for 10 years. Currently he is working as Associate professor at Yogi Vemana University College of Engineering, Kadapa, India. His areas of interest are Numerical Electromagnetics and Fractal antennas.

N. V. S. N. Sarma obtained his Bachelors degree in Engineering with specialization Electronics and Communications Engineering from College of Engineering, Kakinada, Jawahar Lal Nehru Technological University in the year 1984. His Masters and Doctoral degrees are from Indian Institute of Technology, Kharagpur, India in the year 1985 and 1992, respectively. He has been with the Department of Electronics and Communications Engineering at National Institute of Technology, Warangal, India at various positions since 1990. About 30 papers are at his credit in International and National journals and conferences. His areas of interest include Numerical Electromagnetics, Fractal-shaped microstrip antennas, adaptive antenna arrays and Fault diagnosis of phased antenna arrays.